Journal of Energy Chemistry 47 (2020) 256–262

Contents lists available at ScienceDirect

Journal of Energy Chemistry

journal homepage: www.elsevier.com/locate/jechem

http://www.journals.elsevier.com/journal-of-energy-chemistry/

Flame-retarding battery cathode materials based on reversible multi-electron redox chemistry of phenothiazine-based polymer

Jing Lv[a,1], Jing Ye[b,1], Gaole Dai[a], Zhihui Niu[c,*], Yi Sun[d], Xiaohong Zhang[a], Yu Zhao[a,*]

[a] Institute of Functional Nano and Soft Materials (FUNSOM), Jiangsu Key Laboratory for Carbon-Based Functional Materials and Devices, Soochow University, Suzhou 215123, Jiangsu, China
[b] Analytical and Testing Centre, Soochow University, Suzhou 215123, Jiangsu, China
[c] School of Physics and Optoelectronic Engineering, Shandong University of Technology, Zibo 250049, Shandong, China
[d] College of Textile and Clothing Engineering, Soochow University, Suzhou 215123, Jiangsu, China

ARTICLE INFO

Article history:
Received 2 January 2020
Revised 3 February 2020
Accepted 4 February 2020
Available online 25 February 2020

Keywords:
Flame retardancy
Molecular design
Phenothiazine
Batteries
Energy storage

ABSTRACT

Polymeric organic battery materials are promising alternatives to the transition-metal-based ones owing to their enriched chemistries. However, the flammability of organic compounds brings in serious concern on battery safety. In addition to use flame-retarding electrolyte/electrolyte additives or battery separators, flame retardancy can readily be achieved through the integration of flame-retarding unit into the polymer backbone, imparting the flame retardancy permanently. The as-designed polymer based on phenothiazine shows significantly shortened self-extinguished time without deteriorating its intrinsic thermodynamic and electrochemical properties. Moreover, two electron per phenothiazine molecule is realized for the first time in a highly reversible manner with discharge voltages of 3.52 V and 4.16 V versus Li^+/Li and an average capacity of ca. 120 mAh g^{-1} at a current rate of 2 C. The origin of the reversibility is investigated through density functional theory (DFT) calculations. These findings address the importance of molecular design for safer and more stable organic materials for batteries.

1. Introduction

Organic battery materials are considered as promising alternatives to the transition-metal-based ones owing to their enriched chemistries that operate beyond the principle of current rechargeable batteries [1]. Other benefits of organic battery materials include their lower toxicity and production cost compared to inorganic compounds, and the potential that they can be made from sustainable precursors [2,3]. Many types of organic compounds potentially suitable for battery applications have been intensively investigated, such as derivatives of redox-active single molecules [4–12] and macromolecules, especially the polymers [13–18]. One of the major challenges toward their further implementation may arise from the flammability of organic compounds, which brings in serious concern on battery safety, and is of particular concern among government regulatory bodies, manufacturers and consumers alike upon commercialization [19–22]. The common strategies to enhance the battery safety usually relies on the use of flame-retarding electrolyte/electrolyte additives [23–25], the modification of separators [26,27] or binder [28,29] to make them uninflammable (Fig. 1(a)). In fact, the electrode materials consume much more weight fraction than the other components in a conventional Li-ion cell [21,30]. And using active materials with reasonably high weight fraction benefits the development of high-energy batteries. Therefore, to alleviate the safety concern arising from the flammable cell components, it is utmost important to make the active material uninflammable, which represents a pivotal part of the development and application of organic batteries.

Polymer combustion produces volatile polymer fragments, which diffuse into the flame zone and react with oxygen by free-radical chain process to yield radicals with complex composition (Fig. 1(b)) [31]. As one of the most widely used flame-retarding materials, halogens decompose to HX upon combustion, and the generated HX further decompose to X• radicals. The generated HX and X• radicals serve as flame-retardant to extinguish H•, OH• and O• radicals, which are involved in the major heat release reactions during combustion (Fig. 1(c)). For polymeric battery materials, flame retardancy can be achieved through the integration of either

* Corresponding authors.
E-mail addresses: niuzh@sdut.edu.cn (Z. Niu), yuzhao@suda.edu.cn (Y. Zhao).
[1] These authors contributed equally to this work.

https://doi.org/10.1016/j.jechem.2020.02.017

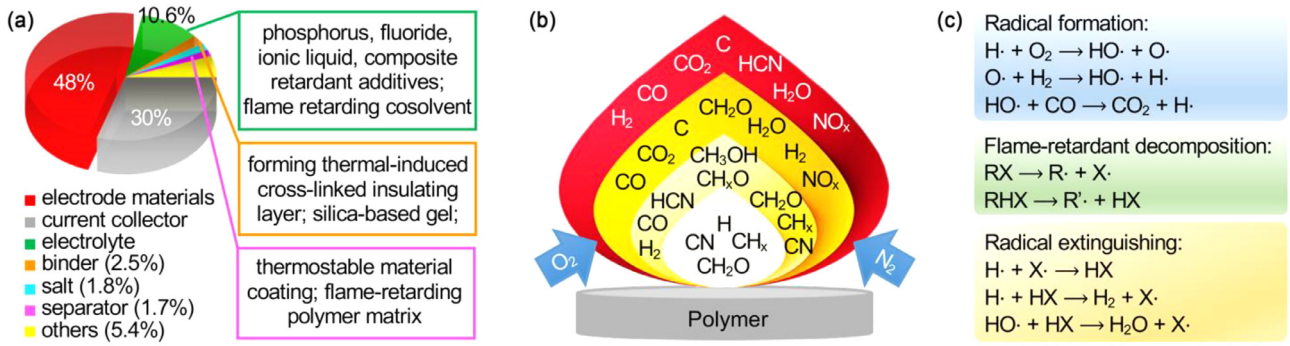

Fig. 1. (a) Typical material mass percent for a battery pack in an electrical vehicle and common strategies for flame-retardancy of battery components [30]. (b) Representative species in a typical flame and (c) the major reactions involved during flame-retarding process.

additive-type or reactive-type flame-retarding unit into the corresponding polymers [32]. The former incorporates flame-retarding additives into the polymers by physical means, which, in principle, functions similar with the flame-retarding electrolyte/electrolyte additives, and provides the most economical and expeditious way of promoting flame retardancy [33]. However, one must take into consideration of the risks like leaching, degradation, compatibility with the active materials, and potential side reactions upon cell operation. The latter involves the design of new polymeric battery materials with a flame retarding unit either in the chain or as a pendent group. For the sake of stability, it is preferable to covalently incorporate the flame- retarding unit into the polymer backbone so as to imparts the flame retardancy permanently while keeping the original physical and mechanical properties unchanged [34].

Herein, we present the flame-retarding organic battery materials in respond to the increasing safety awareness in the battery-related research. As an example, a polymer based on phenothiazine, which is first used in Li-ion batteries as a redox shuttle for overcharge protection [35,36], is designed and synthesized with incorporation of 4-bromostyrene as the flame-retarding unit and 1,4-divinylbenzene as the crosslinker, which in turn effectively reduces the combustibility of the as-synthesized polymer and improves the integrity of the polymer chains against dissolution. The incorporation of flame-retarding unit into the polymer backbone significantly shortens the self-extinguished time without deteriorating its intrinsic thermodynamic and electrochemical properties. Moreover, the two successive, one-electron transfer processes in a highly reversible manner are realized in phenothiazine, of which the dication state is generally recognized as irreversible [37,38]. The polymer exhibits competitive potentials of 3.52 V and 4.16 V versus Li^+/Li and good cycling performance with an average capacity of ca. 120 mAh g^{-1} at a current rate of 2 C, endowing a galvanometric energy density of ca. 450 Wh kg^{-1}. Besides, the origin of the reversibility is likely due to the substituent of phenyl group that contributes to stabilize the aromatic structure and regulates the energy level of frontier molecular orbitals against potential side reactions in electrolyte.

2. Experimental

2.1. Synthesis of 4-vinylphenyl-phenothiazine (VPPT)

A mixture of phenothiazine (0.398 g, 2 mmol, 98%), 4-bromostyrene (0.402 g, 2.2 mmol, 96%), Cs_2CO_3(1.96 g, 3 mmol, 99.9%), $Pd(OAc)_2$ (22.4 mg, 5 mol%, 99.9%) and XPhos (95 mg, 10 mol%, 99%) was dissolved in toluene (anhydrous, 20 mL) and degassed by three freeze–pump–thaw cycles. The mixture was stirred and heated to reflux overnight. After cooling to room temperature, the mixture was extracted twice with dichloromethane (70 mL). The combined organic phase was washed twice with brine (70 mL). The organic phase was dried over anhydrous Na_2SO_4 (2.0 g, 99%) and the organic solvent was removed under reduced pressure. The crude product was purified by column chromatography to afford the product VPPT. The product was further purified by crystallization in dichloromethane/methanol mixture solvent to give pure VPPT. The total yield was ca. 90% (0.54 g). ^{1}H NMR (600 MHz, d_6-DMSO), δ (ppm) = 7.72 (d, J = 8.2 Hz, 2H), 7.35 (d, J = 8.2 Hz, 2H), 7.06 (dd, J = 7.6, 1.5 Hz, 2H), 6.92 (t, J = 7.8 Hz, 2H), 6.86 – 6.79 (m, 3H), 6.20 (d, J = 8.2 Hz, 2H), 5.91 (d, J = 17.7 Hz, 1H), 5.35 (d, J = 11.0 Hz, 1H); MS (MALDI-TOF): calc for $C_{20}H_{15}NS$, 301.09; found: 301.135.

2.2. Synthesis of 1,4-divinylbenzene

Potassium tert-butoxide (2.69 g, 24 mmol) was added to a solution of methyltriphenylphosphonium bromide (4.28 g, 12 mmol) in tetrahydrofuran (20 mL) at 0 °C and the mixture was stirred for 20 min at room temperature under a nitrogen atmosphere. Afterwards, a solution of terephthaladehyde (0.4 g, 3 mmol) in dry tetrahydrofuran (10 mL) was added dropwise. The mixed solution was then stirred for 1 h and poured onto iced water (120 mL), and extracted twice with hexanes (50 mL). Then, the combined organic phases were washed with brine (ca. 200 mL). The organic phase was dried over anhydrous Na_2SO_4 (2.0 g, 99%) and the organic solvent was removed under reduced pressure. Finally, the crude product was purified using flash chromatography as a light-yellow oil (68% yield, 0.265 g). ^{1}H NMR (600 MHz, Chloroform-d), δ (ppm) = 7.39 (s, 4H), 6.72 (dd, J = 17.6, 10.9 Hz, 2H), 5.77 (dd, J = 17.6, 0.9 Hz, 2H), 5.26 (dd, J = 10.9, 0.9 Hz, 2H).

2.3. Synthesis of poly(4-bromophenyl-phenylphenothiazine) (p-BrPhPT)

The as-synthesized VPPT (903 mg, 3 mmol), 4-bromostyrene (32 mg, 0.17 mmol) and 1,4-divinylbenzene (19 mg, 0.15 mmol, 99%) was added into degassed tetrahydrofuran (anhydrous, 2.0 mL, 99%) and stirred to form the precursor solution. 2,2′-azobisisobutyronitrile (15 mg, 0.09 mmol, 99%) was added into degassed tetrahydrofuran (1.0 mL) to form the radical initiator solution. The radical initiator solution was slowly added into the precursor solution under constant stirring. The resultant solution was added into a flask and immersed in a preheated oil bath. The flask was maintained at 65 °C for 24 h under constant stirring. The polymerization was quenched by adding methanol (5 mL). After cooling to room temperature, the mixture was filtered. The crude product

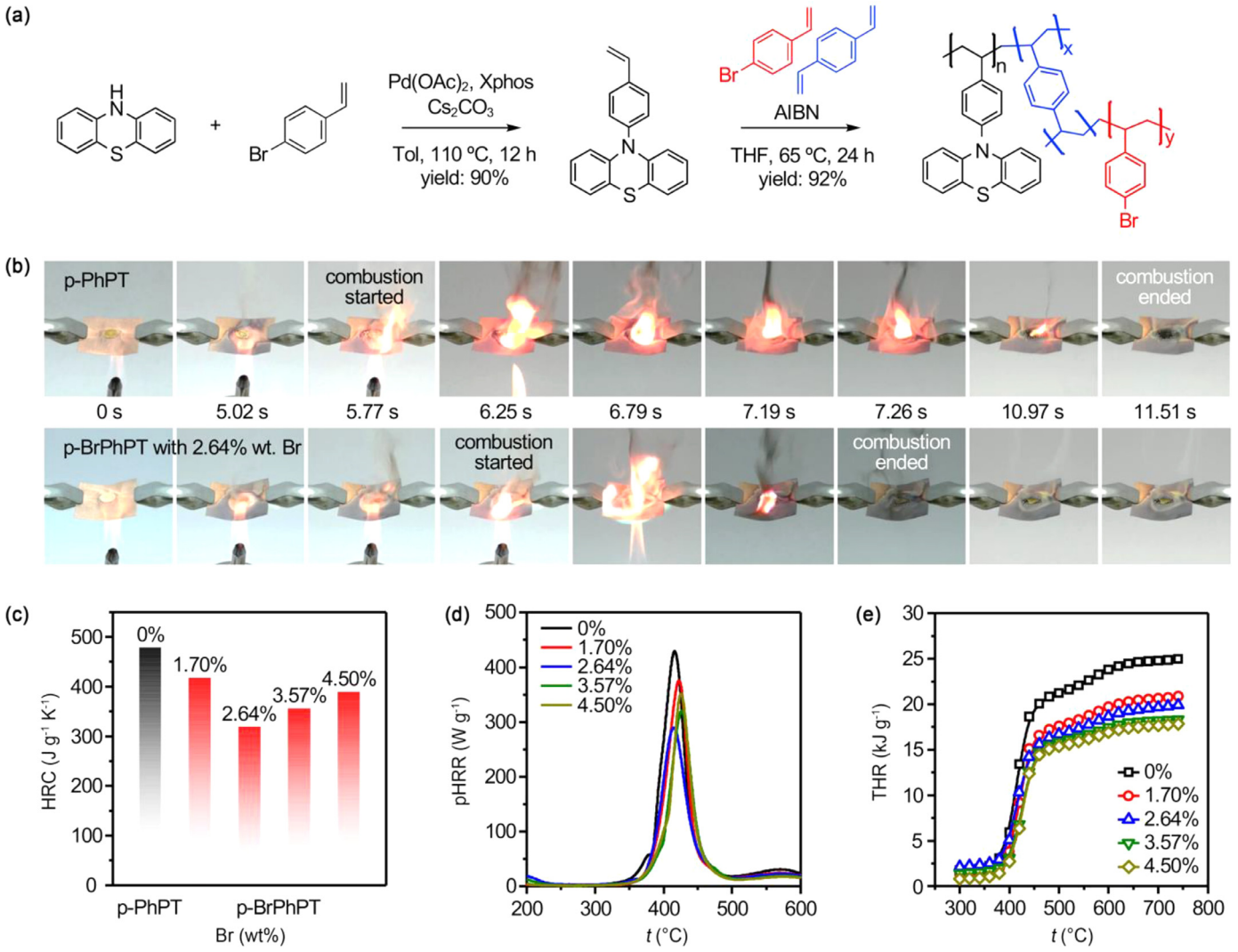

Fig. 2. Fire-safety performance of p-BrPhPT. (a) Synthesis of p-BrPhPT. (b) Visualized demonstration of the combustion process with time for p-PhPT (upper panel) and p-BrPhPT with 2.64%. Br (wt%) (lower panel). (c) HRC, (d) HRR and (e) THR curves obtained from micro combustion calorimetry using p-BrPhPT with Br weight ratio of 0, 1.70%, 2.64%, 3.57% and 4.50%.

was re-dispersed in dichloromethane under ultrasonic wave, and further filtered and washed with dichloromethane and methanol to give the pre-purified product. The pre-purified product was further purified in a home-built Physical Vapor Deposition (PVD) instrument under vacuum ($< 10^{-3}$ Pa) at 300 °C to remove small molecule weight products to give the final product p-BrPhPT. The total yield was ca. 92% (0.88 g).

2.4. Computational details

DFT simulations were performed using the G09 software package. The geometry structure optimization and aromaticity were simulated at the level of B3lyp/6-31G(d,p) [39–43]. NICS values were calculated using the standard GIAO(NMR = GIAO) [44]. To obtain best NICS aromaticity index, NICS(1)zz values were selected [45–47]. Anisotropy of the ACID plots (default isovalue = 0.05 a.u.) was calculated by using the method developed by Herges' group [48]. Spin density was calculated at UB3LYP/6-31G(d,p) level using the non-restrictive open-shell method to eliminate the possibility of spin-polarized singlet state in the +2 valence state with guess = mix to break the symmetry of frontier molecular orbitals. The frontier molecular orbital was calculated considering the electrostatic interaction between cations and PF_6^- in the electrolyte.

3. Results and discussion

The synthetic routes of poly(4-bromophenyl-phenylphenothiazine) (denoted as p-BrPhPT) are shown in Fig. 2(a) (details can be found in the Experimental Section). Pd-catalyzed amination between phenothiazine and 4-bromostyrene afforded 4-vinylphenylphenothiazine (denoted as VPPT) in a high yield of ca. 90% (structural identification is provided in Figs. S1–S3). Free-radical polymerization of VPPT with 4-bromostyrene and 1,4-divinylbenzene using 2,2′-azobisisobutyronitrile (AIBN) as radical initiator afforded cross-linked p-BrPhPT in ca. 92% yield. The molar ratio of VPPT and 1,4-divinylbenzene was fixed to 20:1, and the weight ratio of 4-bromostyrene was adjusted in the range of 1%–7% with respected to the total weight of VPPT and 1,4-divinylbenzene. It should be noted that the molar ratio of the three reactants for copolymerization did not necessarily guarantee the same molar ratio in the final p-BrPhPT. Elemental analysis revealed that phenothiazine was in dominant with weight ratio nearly 90% when the weight ratio of 4-bromostyrene was below 3% (Table S1). Increasing 4-bromostyrene to 5% and 7% resulted in a decreased phenothiazine ratio of ca. 83%. The actual weigh ratio of Br in p-BrPhPT was determined to be 1.70%, 2.64%, 3.57% and 4.50% when using 1 wt%, 3 wt% 5 wt% and 7 wt% 4-bromostyrene, respectively.

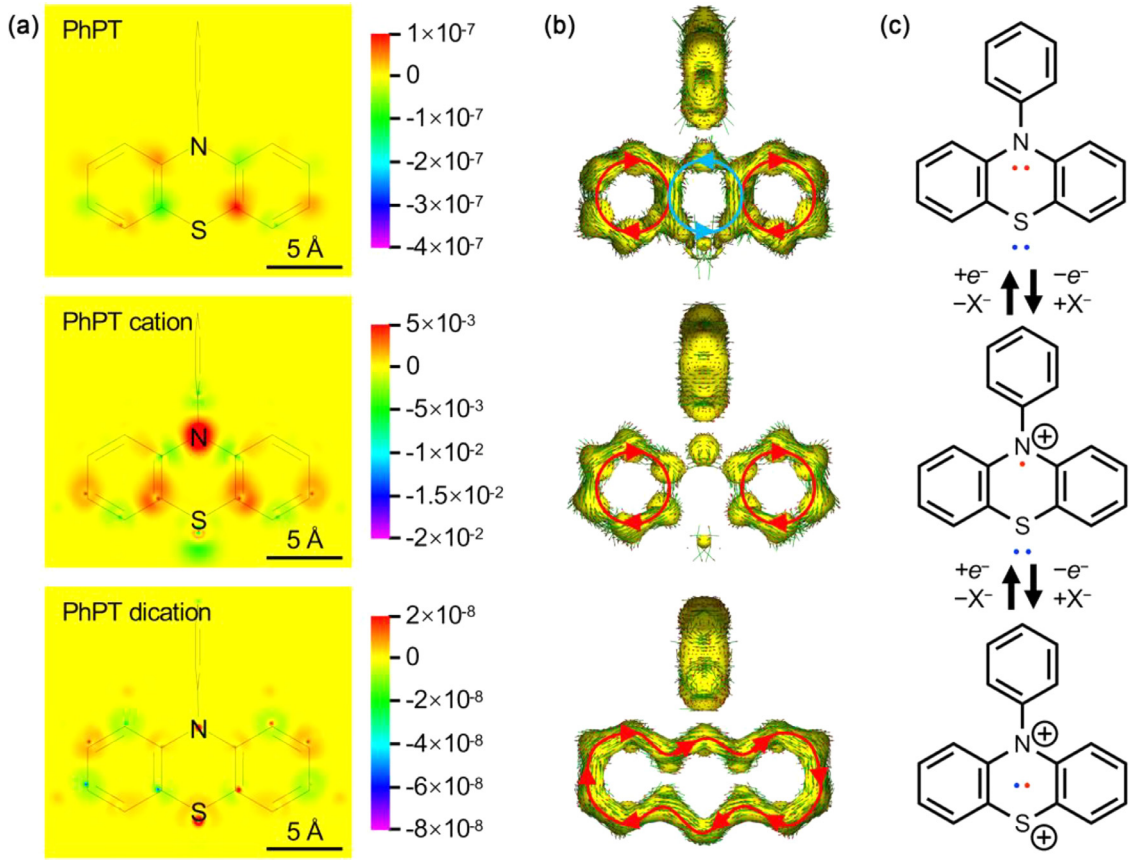

Fig. 3. Redox properties of PhPT. (a) ESD and (b) AICD of PhPT, PhPT cation and PhPT dication. The ACID reflects the π effects only. The basal plane of PhPT is placed perpendicular to the magnetic field vector. Small green arrows are computed current density vectors. The red circles labeled by arrows reflect the global ring current flow direction. (c) Redox mechanism of PhPT. X^- stands for an anion (BF_4^-, PF_6^-, ClO_4^-, etc.) to balance the charge.

Thermogravimetric (TG) and differential scanning calorimetry (DSC) analysis revealed that p-BrPhPT was thermally stable up to 320 °C in air and 350 °C in nitrogen (Fig. S4), and there's no phase change in the temperature range of 25−300 °C (Fig. S5) regardless of the amount of flame-retarding unit, similar with p-PhPT (p-BrPhPT without flame-retarding unit), indicating the thermodynamic properties were not affected upon the incorporation of flame-retarding unit. Notably, p-BrPhPT synthesized with Br weight ratio of 2.64% was able to maintain a high specific capacity of ca. 160 mAh g^{-1} (assuming a two-electron oxidation per each phenothiazine unit would occur in the redox reactions), compared with phenothiazine molecule, of which the theoretical capacity is 178 mAh g^{-1}. Nevertheless, a remarkable improvement in flame retardancy could be achieved in p-BrPhPT without sacrificing its specific capacity.

To demonstrate the self-extinguishing performance, burning test was carried out on as-synthesized p-BrPhPT and p-PhPT. p-BrPhPT started to combust after ignited for 6.25 s, and then self-extinguished within ca. 1 s (Fig. 2(b)). In contrast, p-PhPT was barely self-extinguished after ignition, the combustion time was ca. 5.6 times longer than that of p-BrPhPT. Besides, p-PhPT was almost exhausted during the combustion, while a lot of residuals remained in the case of p-BrPhPT. Further quantitative analysis of micro combustion calorimetry, which is based on the principle of oxygen consumption to mimic a real burning scenario, was performed to evaluate the fire safety of the as-synthesized p-BrPhPT. The heat release capacity (HRC), which is an important factor to determine the fire safety and flame retardancy of polymeric materials, was first measured using p-BrPhPT with Br weight ratio of 0%, 1.70%, 2.64%, 3.57% and 4.50% (Fig. 2(c)). It's found that p-BrPhPT generally showed lower HRC when flame-retarding unit were incorporated. The lowest HRC was achieved at p-BrPhPT with 2.64 wt% of Br. The peak heat release rate (pHRR, Fig. 2(d)) showed a similar tendency with the HRC. In particular, p-BrPhPT with 2.64 wt% Br exhibited the lowest pHRR. Incorporating more flame-retarding units did not further lower the pHRR or THR because of the limited effect on inhibiting the heat release [49–51]. Compared with p-PhPT, p-BrPhPT with 2.64 wt% Br showed a significant 32.7% pHRR decrease. While the total heat release (THR, Fig. 2(e)) decreased with the increase of flame-retarding unit. p-BrPhPT with Br weight ratio of 2.64% and 4.50% exhibited a decrease of 22.3% and 30.1% THR, respectively.

Density Functional Theory (DFT) calculation was applied to reveal the electronic configuration of PhPT intermediates during redox reactions. The electronic spin density (ESD) distribution of PhPT (Fig. 3(a) and Table S2) suggested that only the PhPT cation exhibited strong positive spin density around nitrogen atom [52], while the neutral PhPT and PhPT dication exhibited no single electron free radical character. Both of the anisotropy of the induced current density (AICD, Fig. 3(b)) and nucleus independent chemical shift [17,45,52–55] (NICS(1)zz, Fig. S6) revealed that the benzene rings on both sides of N-S heterocyclic ring showed strong aromatic characteristic considering the negative values with negligible changes and the clockwise circulation of three valence states. For the central N-S heterocyclic ring, the aromaticity changed from anti-aromatic with positives NICS(1)zz values (9.37 ppm) and anticlockwise circulation of neutral PhPT, to almost nonaromatic with small NICS(1)zz values (−1.08 ppm) and no circulation of the PhPT cation, and to aromatic with negative NICS(1)zz values (−25.57 ppm) and clockwise circulation of PhPT dication. Such

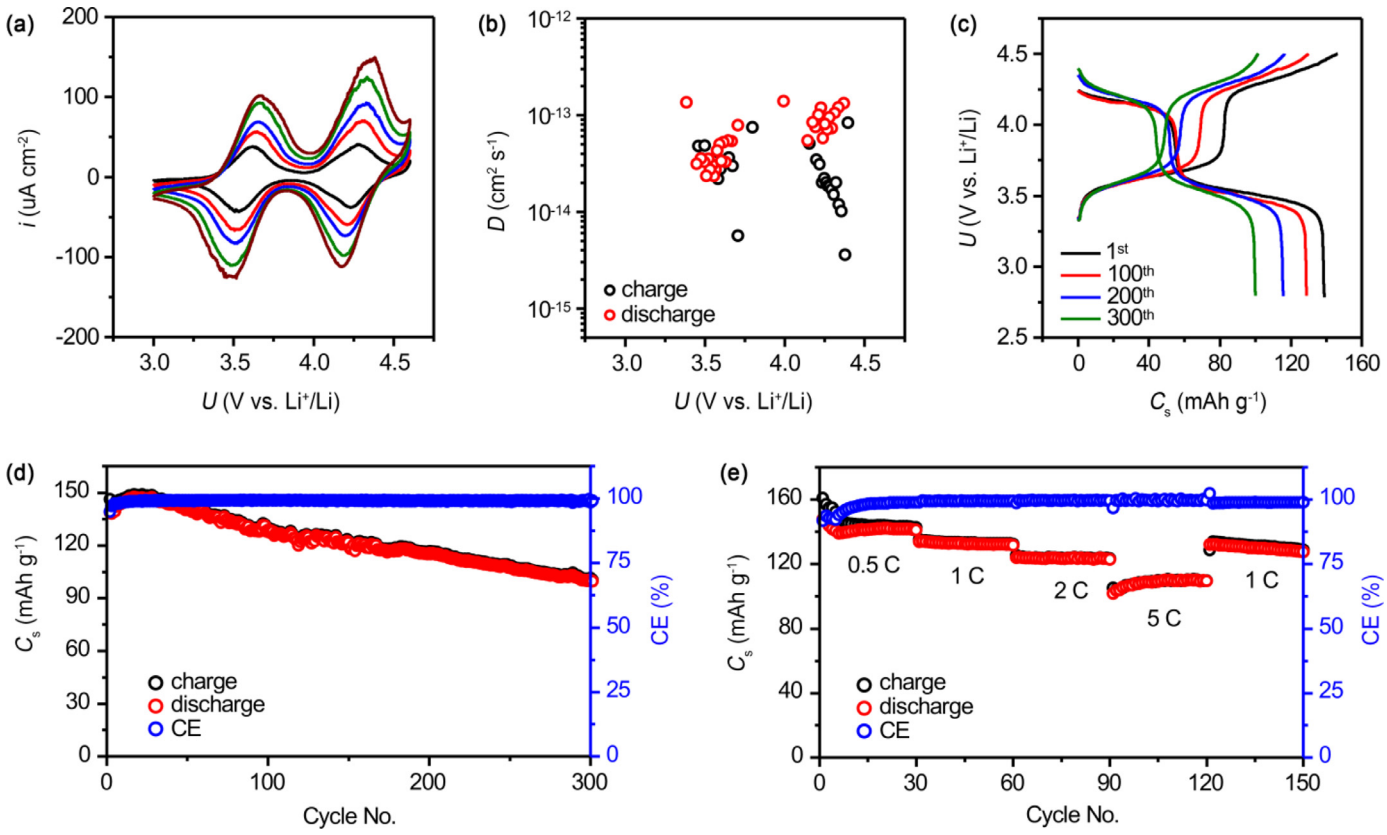

Fig. 4. Electrochemical properties of p-BrPhPT with Br weight ratio of 2.64%. (a) CV profiles at different sweeping rates of 0.2, 0.4, 0.6, 0.8 and 1.0 mV s^{-1} in the potential range of 3.0 – 4.6 V vs. Li^+/Li. (b) Diffusion coefficient as a function of potential during the charge-discharge processes. The diffusion coefficient is calculated based on three runs. (c) Charge-discharge profiles, (d) cycling performance and corresponding Coulombic efficiency, and (e) rate performance of a p-BrPhPT | Li cell. All tests were carried out in a CR2032 coin cell. The electrolyte is EC/DEC containing 1 M $LiPF_6$. More details of testing conditions are provided in the expanded experimental section in the Supporting Information.

an antiaromatic-aromatic transformation revealed that both PhPT cation and dication were thermodynamically stable. Furthermore, the frontier molecular orbital and orbital composition analysis (Fig. S7) demonstrated that the π electrons of N and S atom are indubitable as the active sites for the first and second redox reaction, which is in consistent with the former aromaticity analysis. The electrochemical process upon oxidation should involve the first loss of one beta π-electron of N to form PhPT cation, and the second loss of one alpha π-electron of S to form PhPT dication, in which the remaining alpha π-electron of N and beta π-electron of S occupy the same orbital in the conjugated structure (Fig. 3(c)). Except for the effects of conjugation and electronic delocalization, the structural change during the electrochemical processes have also been studied. During the oxidation of the cathode, the PF_6^-

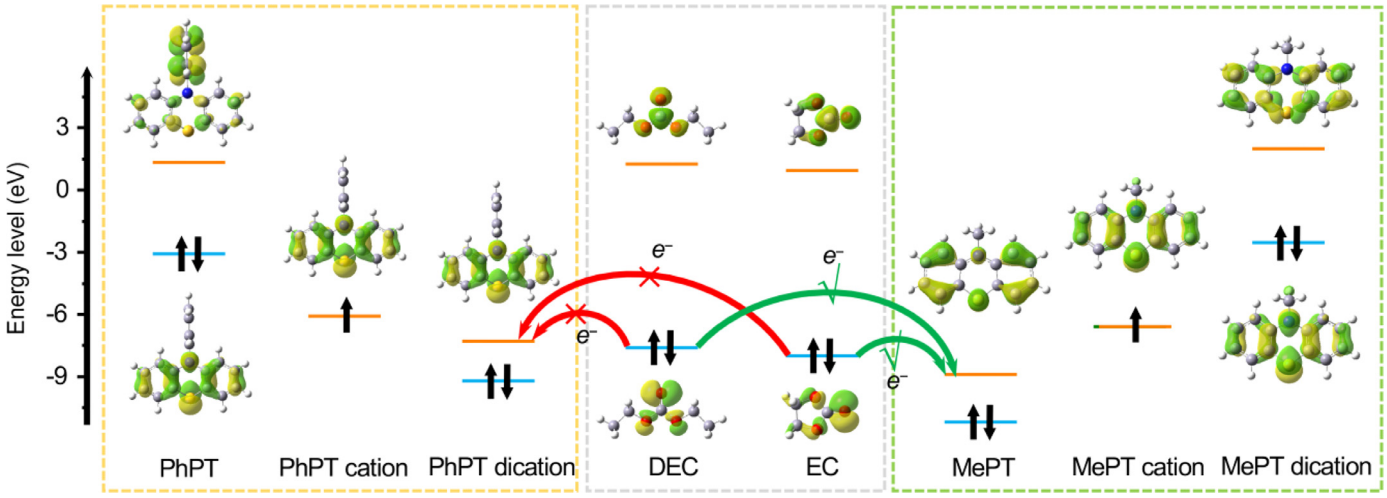

Fig. 5. Frontier molecular orbital and corresponding energy level of PhPT, electrolyte molecules (DEC and EC), and MePT. Note that the energy states of PhPT change with the oxidation due to the relaxation effect of the molecules.

ions would diffusion into the cathode to neutralize the PhPT moiety cations, the PF_6^- prefer to bind with the N and S redox centers of PhPT, which exhibit the most positive charges according to molecular surface electrostatic potential calculation (Fig. S8), and the PF_6^- as the charge carriers can balance charges when happening redox reaction through binding to the central N and S atoms of PhPT with the most positive charges and keep stable configurations without large structural distortion.

Such a successive two-step, one-electron redox reaction was verified by cyclic voltammogram (CV) as shown in Fig. 4(a). Two pairs of cathodic and anodic peaks with high symmetry were observed. The redox peaks centered at 3.57 V and 4.25 V vs. Li^+/Li were assigned to the redox reaction occurred at N and S, respectively. The redox reactions were electrochemically reversible as evident by the small peak separation of ca. 78 mV for N and 47 mV for S at a sweeping rate of 0.2 mV s^{-1}. The peak current was in proportion to the square root of the sweeping rate (Fig. S9), indicating the electrochemical process was diffusion-controlled [17,52]. The diffusion coefficient of PF_6^- in p-BrPhPT was measured using galvanostatic intermittent titration technique (GITT, more details are provided in the expanded experimental section in the Supporting Information), and determined to be 10^{-14} – 10^{-12} cm^2 s^{-1} (Fig. 4(b) and Fig. S10), which is in the same order of magnitude with most battery materials [17,56–57]. Fig. 4(c) shows the 1st, 100th, 200th and 300th charge-discharge profiles of a p-BrPhPT | Li cell with low voltage hysteresis at a current rate of 2 C (320 mA g^{-1}). The average discharge voltage was 3.52 V and 4.16 V vs. Li^+/Li, in accordance with the CV measurement. Two plateaus were clearly observed even at extended cycles, suggesting the N and S redox centers were highly stable and reversible. The corresponding capacity from N was slightly higher than that from S. This phenomenon was also observed when the cell was cycled in the potential range of each plateau (Figs. S11 and S12). This was possibly resulted from the high voltage of 4.2 – 4.5 V vs. Li^+/Li, in which the carbonate electrolyte may start to decompose and trigger the side reactions with the active material [14,58]. The initial discharge capacity reached 137 mAh g^{-1}, ca. 85% of the theoretical capacity (ca. 160 mAh g^{-1}), and maintained ca. 101 mAh g^{-1} in 300 cycles (Fig. 4(d)). Similar cycling performance was observed in the cell using a p-PhPT cathode (Fig. S13). The slightly increased specific capacity should arise from the increased weight fraction of phenothiazine, indicating that the flame-retarding units showed little effect on the cyclability of p-BrPhPT. Notably, the corresponding Coulombic efficiency reached 93% in the initial cycle, and remained in the range between 99% and 99.8% in the rest cycles. Such a high initial Coulombic efficiency should be contributed from the covalently crosslinked frameworks that greatly suppresses the dissolution of the active material in the electrolyte. UV data indicated that the solubility of the polymer decreased after adding the crosslinker. The corresponding absorption peak was invisible or beyond the detection limit of the equipment for a saturated p-BrPhPT EC/DEC solution (Fig. S14). Power performance suggested the p-BrPhPT electrode was able to deliver an average capacity of 140, 132, 123 and 110 mAh g^{-1} at a current rate of 0.5, 1, 2 and 5 C, respectively, with high Coulombic efficiency (Fig. 4(e)).

To understand the origin of the reversibility from the redox reaction of S, the chemical stability of PhPT, PhPT cation and PhPT dication in the given carbonate-based electrolyte was investigated as summarized in Fig. 5 [59]. It was observed that the energy levels of the lowest unoccupied molecular orbital (LUMO) of PhPT and PhPT dication and the singly occupied molecular orbital (SOMO) of the PhPT cation were higher than the highest occupied molecular orbital (HOMO) level of EC/DEC. More importantly, the LUMO levels of PhPT, PhPT cation and PhPT dication were located above the HOMO level of EC/DEC, indicating that the electron transfer from DEC/EC to PhPT in any oxidation state during the electrochemical processes inside a cell is thermodynamically unfavourable. Similarly, the electron transfer from PhPT, PhPT cation or PhPT dication to EC/DEC was also energetically limited, because the HOMO/SOMO levels of PhPT, PhPT cation or PhPT dication were lower than the LUMO levels of EC/DEC. For comparison, N-methylphenothiazine (denoted as MePT), of which the S atom was believed to be electrochemically irreversible [37,38], was investigated. It's found that the LUMO energy level of MePT dication was lower than the HOMO energy level of DEC/EC, implying that the electron transfer from DEC/EC to MePT dication was thermodynamically favourable. Such electron transfer would benefit the side reaction to occur between MePT dication and the electrolyte molecules, thus significantly weakening reversibility of MePT. Besides, through the analysis on the structure parameters and Mayer bond order (Table S3), the π-electron conjugate effect of phenyl-substitute phenothiazine also showed better electronic delocalization and structure stability than methyl-substitute phenothiazine, in which the weak bond strength of H_3C–N in MePT dication is very likely to undergo demethylation [16]. To take full usage of N and S redox centre in phenothiazine-based cathode materials or electrolyte additives for overcharge protection, it's highly desirable to use phenyl group instead commonly used methyl group as the substituent for the sake of structural stability and electrochemical reversibility.

4. Conclusions

In conclusion, to address the challenge arising from inflammable organic battery materials, self-extinguishing phenothiazine-based polymer is designed and synthesized with 4-bromostyrene as the flame-retarding unit and 1,4-divinylbenzene as the crosslinker. Surprisingly, the phenothiazine unit is found to be highly reversible either using N or S as the redox center, though the latter is generally recognized as electrochemically irreversible. The greatly improved reversibility should stem from the substituent of phenyl group, which contributes to stabilize the aromatic structure and regulates the energy level of frontier molecular orbitals against potential side reactions in electrolyte. The as-synthesized p-BrPhPT thus exhibits highly reversible multi-electron redox chemistry, resulting in high discharge voltage of 3.52 V and 4.16 V versus Li^+/Li and an average capacity of ca. 120 mAh g^{-1} at a current rate of 2 C. We believe flame-retarding active materials are essential for building a safer battery, and proper molecular modification on these materials may advance the organic batteries further towards high capacity and reliability.

Declaration of Competing Interest

We declare no competing interest.

Acknowledgments

We acknowledge financial support from the National Natural Science Foundation of China (grant no. 51772199), the Natural Science Foundation of Jiangsu Province (Grant no. BK20170329), the Collaborative Innovation Center of Suzhou Nano Science & Technology, the Priority Academic Program Development of Jiangsu Higher Education Institutions, and the 111 Project.

Supplementary materials

Supplementary material associated with this article can be found, in the online version, at doi:10.1016/j.jechem.2020.02.017.

References

[1] S. Muench, A. Wild, C. Friebe, B. Häupler, T. Janoschka, U.S. Schubert, Chem. Rev. 116 (16) (2016) 9438–9484.
[2] D. Larcher, J.M. Tarascon, Nat. Chem. 7 (1) (2015) 19–29.
[3] T.B. Schon, B.T. McAllister, P.F. Li, D.S. Seferos, Chem. Soc. Rev. 45 (22) (2016) 6345–6404.
[4] B.T. McAllister, L.T. Kyne, T.B. Schon, D.S. Seferos, Joule 3 (3) (2019) 620–624.
[5] S. Lee, G. Kwon, K. Ku K. Yoon, S.-.K. Jung, H.-.D. Lim, K. Kang, Adv. Mater. 30 (42) (2018) 1704682.
[6] C. Peng, G.H. Ning, J. Su, G. Zhong, W. Tang, B. Tian, C. Su, Di. Yu, L. Zu, J. Yang, M.F. Ng, Y.S. Hu, Y. Yang, M. Armand, K.P. Loh, Nat. Energy 2 (7) (2017) 17074.
[7] Y. Liang, Y. Jing, S. Gheytani, K.Y. Lee, P. Liu, A. Facchetti, Y. Yao, Nat. Mater. 16 (8) (2017) 841–848.
[8] J.D. Milshtein, A.P. Kaur, M.D. Casselman, J.A. Kowalski, S. Modekrutti, P.L. Zhang, N. Harsha Attanayake, C.F. Elliott, S.R. Parkin, C. Risko, F.R. Brushett, S.A. Odom, Energy Environ. Sci. 9 (11) (2016) 3531–3543.
[9] B. Häupler, A. Wild, U.S. Schubert, Adv. Energy Mater. 5 (2015) 1402034.
[10] M. Armand, S. Grugeon, H. Vezin, S. Laruelle, P. Ribière, P. Poizot, J.M. Tarascon, Nat. Mater. 8 (2) (2009) 120–125.
[11] Y. Ding, Y. Li, G. Yu, Chem 1 (5) (2016) 790–801.
[12] B. Tian, Z. Ding, G.H. Ning, W. Tang, C. Peng, B. Liu, J. Su, C. Su, K.P. Loh, Chem. Commun. 53 (20) (2017) 2914–2917.
[13] M. Kolek, F. Otteny, J. Becking, M. Winter, B. Esser, P. Bieker, Chem. Mater. 30 (18) (2018) 6307–6317.
[14] M. Lee, J. Hong, B. Lee, K. Ku, S. Lee, C.B. Park, K. Kang, Green Chem. 19 (13) (2017) 2980–2985.
[15] M. Kolek, F. Otteny, P. Schmidt, C. Mück-Lichtenfeld, C. Einholz, J. Becking, J. Schleicher, M. Winter, P. Bieker, B. Esser, Energy Environ. Sci. 10 (11) (2017) 2334–2341.
[16] A. Wild, M. Strumpf, B. Häupler, M.D. Hager, U.S. Schubert, Adv. Energy Mater. 7 (5) (2016) 1601415.
[17] Z. Niu, H. Wu, L. Liu, G. Dai, S. Xiong, Y. Zhao, X. Zhang, J. Mater. Chem. A 7 (17) (2019) 10581–10588.
[18] P. Acker, L. Rzesny, C.F.N. Marchiori, C.M. Araujo, B. Esser, Adv. Funct. Mater. 29 (45) (2019) 1906436.
[19] J.B. Goodenough, Energy Storage Mater. 1 (2015) 158–161.
[20] L. Lu, X. Han, J. Li, J. Hua, M. Ouyang, J. Power Sources 226 (2013) 272–288.
[21] P. Ribière, S. Grugeon, M. Morcrette, S. Boyanov, S. Laruelle, G. Marlair, Energy Environ. Sci. 5 (1) (2012) 5271–5280.
[22] J.B. Goodenough, Y. Kim, J. Power Sources 196 (16) (2011) 6688–6694.
[23] Q. Wang, L. Jiang, Y. Yu, J. Sun, Nano Energy 55 (2019) 93–114.
[24] J. Wang, Y. Yamada, K. Sodeyama, E. Watanabe, K. Takada, Y. Tateyama, A. Yamada, Nat. Energy 3 (1) (2017) 22–29.
[25] S.S. Zhang, J. Power Sources 162 (2) (2006) 1379–1394.
[26] K. Liu, W. Liu, Y. Qiu, B. Kong, Y. Sun, Z. Chen, D. Zhuo, D. Lin, Y. Cui, Sci. Adv. 3 (1) (2017) 1601978.
[27] K. Ozawa, Solid State Ionics 69 (3–4) (1994) 212–221.
[28] G. Zhou, K. Liu, Y. Fan, M. Yuan, B. Liu, W. Liu, F. Shi, Y. Liu, W. Chen, J. Lopez, D. Zhuo, J. Zhao, Y. Tsao, X. Huang, Q. Zhang, Y. Cui, ACS Cent. Sci. 4 (2) (2018) 260–267.
[29] Y. Wu, Lithium-ion batteries: Fundamentals and Applications, CRC Press, Boca Raton, FL, 2015.
[30] B.A. Johnson, R.E. White, J. Power Sources 70 (1) (1998) 48–54.
[31] G.L. Nelson, Fire and Polymers II: Materials and Tests For Hazard prevention, ACS Symposium Series, American Chemical Society, Washington DC, 1995.
[32] D.K. Chattopadhyay, D.C. Webster, Prog. Polym. Sci. 34 (10) (2009) 1068–1133.
[33] L. Liu, Y. Xu, M. Xu, Z. Li, Y. Hu, B. Li, Compos. Part B Eng. 167 (2019) 422–433.
[34] M. El Gouri, A. El Bachiri, S.E. Hegazi, M. Rafik, A. El Harfi, Polym. Degrad. Stab. 94 (11) (2009) 2101–2106.
[35] C. Buhrmester, L. Moshurchak, R.L. Wang, J.R. Dahn, J. Electrochem. Soc. 153 (2006) 288–294.
[36] L.M. Moshurchak, C. Buhrmester, R.L. Wang, J.R. Dahn, Electrochim. Acta 52 (11) (2007) 3779–3784.
[37] J.A. Kowalski, M.D. Casselman, A.P. Kaur, J.D. Milshtein, C.F. Elliott, S. Modekrutti, N.H. Attanayake, N. Zhang, S.R. Parkin, C. Risko, F.R. Brushett, S.A. Odom, J. Mater. Chem. A 5 (46) (2017) 24371–24379.
[38] F. Otteny, M. Kolek, J. Becking, M. Winter, P. Bieker, B. Esser, Adv. Energy Mater. 8 (33) (2018) 1802151.
[39] P.J. Stephens, F.J. Devlin, C.F. Chabalowski, M.J. Frisch, J. Phys. Chem. 98 (45) (1994) 11623–11627.
[40] A.D. Becke, J. Chem. Phys. 98 (7) (1993) 5648–5652.
[41] W.J. Hehre, R. Ditchfield, J.A. Pople, J. Chem. Phys. 56 (5) (1972) 2257–2261.
[42] J.D. Dill, J.A. Pople, J. Chem. Phys. 62 (7) (1975) 2921–2923.
[43] M.M. Francl, W.J. Pietro, W.J. Hehre, J.S. Binkley, M.S. Gordon, D.J. DeFrees, J.A. Pople, J. Chem. Phys. 77 (7) (1982) 3654–3665.
[44] Z. Chen, C.S. Wannere, C. Corminboeuf, R. Puchta, P.v.R. Schleyer, Chem. Rev. 105 (2005) 3842–3888.
[45] H. Wei, Y. Liu, T.Y. Gopalakrishna, H. Phan, X. Huang, L. Bao, J. Guo, J. Zhou, S. Luo, J. Wu, Z. Zeng, J. Am. Chem. Soc. 139 (44) (2017) 15760–15767.
[46] H. Fallah-Bagher-Shaidaei, C.S. Wannere, C. Corminboeuf, R. Puchta, P.v.R. Schleyer, Org. Lett. 8 (5) (2006) 863–866.
[47] Y. Zhu, F. Yang, Z. Niu, H. Wu, Y. He, H. Zhu, J. Ye, Y. Zhao, X. Zhang, J. Power Sources 417 (2019) 83–89.
[48] D. Geuenich, K. Hess, F. Köhler, R. Herges, Chem. Rev. 105 (10) (2005) 3758–3772.
[49] B.W. Liu, L. Chen, D.M. Guo, X.F. Liu, Y.F. Lei, X.M. Ding, Y.Z. Wang, Angew. Chem. Int. Ed. 58 (27) (2019) 9188–9193.
[50] R. Liepins, J.R. Surles, N. Morosoff, V.T. Stannett, J. Appl. Polym. Sci. 21 (9) (1977) 2529–2550.
[51] W. Xing, Y. Hu, L. Song, X. Chen, P. Zhang, J. Ni, Polym. Degrad. Stab. 94 (7) (2009) 1176–1182.
[52] G. Dai, Y. Liu, Z. Niu, P. He, Y. Zhao, X. Zhang, H. Zhou, Matter 1 (4) (2019) 945–958.
[53] Q. Wang, T.Y. Gopalakrishna, H. Phan, T.S. Herng, S. Dong, J. Ding, C. Chi, Angew. Chem. Int. Ed. 56 (38) (2017) 11415–11419.
[54] X. Lu, S. Lee, Y. Hong, H. Phan, T.Y. Gopalakrishna, T.S. Herng, T. Tanaka, M.E. Sandoval-Salinas, W. Zeng, J. Ding, D. Casanova, A. Osuka, D. Kim, J. Wu, J. Am. Chem. Soc. 139 (37) (2017) 13173–13183.
[55] G. Dai, Y. He, Z. Niu, P. He, C. Zhang, Y. Zhao, X. Zhang, H. Zhou, Angew. Chem. Int. Ed. 58 (29) (2019) 9902–9906.
[56] S. Miyoshi, T. Akbay, T. Kurihara, T. Fukuda, A.T. Staykov, S. Ida, T. Ishihara, J. Phys. Chem. C 120 (40) (2016) 22887–22894.
[57] G. Dai, X. Wang, Y. Qian, Z. Niu, X. Zhu, J. Ye, Y. Zhao, X. Zhang, Energy Storage Mater. 16 (2018) 236–242.
[58] S.K. Jung, H. Gwon, J. Hong, K.Y. Park, D.H. Seo, H. Kim, J. Hyun, W. Yang, K. Kang, Adv. Energy Mater. 4 (1) (2014) 1300787.
[59] G. Kwon, S. Lee, J. Hwang, H. Shim, B. Lee, M.H. Lee, Y. Ko, S.-.K. Jung, K. Ku, J. Hong, K. Kang, Joule 2 (9) (2018) 1771–1782.